Astron. Astrophys. 320, 731–745 (1997)

ASTRONOMY AND ASTROPHYSICS

Evidence for a New "Superwind" Galaxy – NGC 4666

Michael Dahlem[1⋆], **Monika G. Petr**[2], **Matthew D. Lehnert**[3,4⋆⋆], **Timothy M. Heckman**[5], **and Matthias Ehle**[6]

[1] Space Telescope Science Institute, 3700 San Martin Drive, Baltimore, MD 21218, USA
[2] Max-Planck-Institut für Astronomie, Königstuhl 17, D-69117 Heidelberg, Germany
[3] Leiden Observatory, P.O. Box 9513, 2300 RA Leiden, The Netherlands
[4] Institute for Geophysics and Planetary Physics, Lawrence Livermore National Laboratory, P. O. Box 808, L-413, Livermore, CA 94551-9900, USA
[5] Johns Hopkins University, Department of Physics and Astronomy, 3400 N. Charles Street, Baltimore, MD 21218-2695, USA
[6] ATNF/CSIRO, P.O. Box 76, Epping, NSW 2121, Australia

Received 18 April 1996 / Accepted 5 September 1996

Abstract. Multi-wavelength observations of the edge-on galaxy NGC 4666 have led to the detection of an outflow cone associated with a galactic superwind, emanating from a central starburst with a radial diameter of about 6.5 kpc. The outflow is traced up to 7.5 kpc above the plane by optical emission line filaments, nonthermal radio continuum emission, associated magnetic fields perpendicular to the galactic plane, and soft X-ray emission from hot gas. Optical spectroscopy exhibits the kinematic signature of an outflow and the observed line ratios indicate that shock heating is the most likely excitation mechanism for the emission line gas. The outflow is well approximated by a 6.5 kpc base (the extent of the central starburst) plus a cone with an opening angle of $30° \pm 10°$.

In the outer disk of NGC 4666 numerous luminous H II regions were detected, which lead to additional outflows (galactic fountains or chimneys) of gas into the halo. Radially the radio halo is much more extended than the central outflow cone and it has an exponential z-scale height at 1.43 GHz of 1.7 ± 0.28 kpc. NGC 4666 is in many respects very similar to NGC 4631, another edge-on galaxy with an extended gaseous halo.

Key words: galaxies: NGC 4666 – galaxies: ISM – galaxies: magnetic fields – galaxies: starburst – radio continuum: galaxies

1. Introduction

Over the past decade it has been found that starburst galaxies have halos of gas which is expelled from their disks by multiple supernova (SN) events creating "superbubbles" (Tomisaka et al. 1981). The breakout of gas from such superbubbles in starbursts into the halos can lead to so-called galactic "superwinds"(see Heckman et al. 1990 [hereafter HAM90]; Lehnert & Heckman 1996). In galaxies like, e.g., NGC 253 and M 82 there is incontrovertable morphological and kinematical evidence for outflows of matter from the central starburst (Lynds & Sandage 1963; Bland & Tully 1988; McKeith et al. 1995; Reuter et al. 1994). The star formation (SF) regions and associated SNe are seen in different wavebands as "knots" or "hot spots" (e.g. Antonucci & Ulvestad 1988; Muxlow et al. 1994; Forbes et al. 1991; Kronberg et al. 1981, 1985).

Recently, evidence has been accumulated that SF in the disks of "normal" late-type spirals can also drive outflows into their halos (e.g. Dettmar 1992 and references therein). For radio synchrotron halos, which are formed by cosmic-rays (CRs) and magnetic fields outside the galaxy disks, Dahlem et al. (1995; hereafter DLG95) have shown that there is a quantitative relation between the level of SF in the galaxy disks and the properties and shapes of the associated radio halos (see also Völk et al. [1989] and Tomisaka [1992]).

NGC 4666 is classified as an Sc galaxy, which has an optical extent of $4\farcm2 \times 1\farcm5$ and an inclination angle of $i = 80°$ (de Vaucouleurs et al. 1991; RC3). In the optical regime NGC 4666 was poorly studied until Lehnert (1992) and Lehnert & Heckman (1995) obtained R-band and Hα+N [II] narrow-band images. These data and new optical spectra obtained by us will be used in the following to study the properties of the warm ionized medium in NGC 4666 in detail.

From the far-infrared (FIR) fluxes listed for NGC 4666 in the IRAS Point Source Catalog (Fullmer & Lonsdale 1989; f_{60} = 37.34 Jy and f_{100} = 82.88 Jy) we calculate an FIR luminosity of $\log L_{FIR}[L_\odot] = 10.69$. This is higher than the values for the two actively star-forming galaxies NGC 253 ($\log L_{FIR}[L_\odot] = 10.22$) and NGC 4631 ($\log L_{FIR}[L_\odot] = 9.90$), which indicates that the global star formation rate (SFR) in NGC 4666 is high.

Send offprint requests to: MD, mdahlem@astro.estec.esa.nl

⋆ Affiliated with the Astrophysics Division in the Space Science Department of ESA; present address: ESTEC, Astrophysics Division, Postbus 299, 2200 AG Noordwijk, The Netherlands

⋆⋆ Visiting Astronomer, Cerro Tololo Inter-American Observatory, National Optical Astronomy Observatories, which is operated by the Association of Universities for Research in Astronomy, Inc., under contract with the National Science Foundation

Table 1. Observations of NGC 4666

Dataset	Instrument	Observing date	Integration time
R-band continuum image	CTIO 1.5-m	May 17 1991	10 min.
Hα+N [II] image	CTIO 1.5-m	May 17 1991	1.0 h
Optical red spectroscopy	Las Campanas 2.5-m	Mar. 02 1990	1.0 h
Optical blue spectroscopy	CTIO 4-m	Mar. 23 1993	1.5 h
4.89 GHz radio continuum	VLA D array	Dec. 20 & 24 1993	12.5 h
1.43 GHz radio continuum	VLA C array	Nov. 20 1994	4 h

Based on its L_{FIR}, $\log(L_{FIR}/L_B) = 0.48$, and its FIR colour of $f_{60}/f_{100} = 0.45$, NGC 4666 is a typical FIR-selected galaxy (see Table 1 by Lehnert & Heckman 1995). This and our earlier result that the properties of gaseous halos of galaxies depend on the level of SF in their disks (DLG95) makes NGC 4666 a good candidate to search for halo emission in different wavebands.

The new radio data presented here are much more sensitive (by factors of about 5 [4.89 GHz] and 3 [1.43 GHz]) than those obtained by Sukumar et al. (1988; hereafter SVK), who found a first indication of a radio halo in NGC 4666. In addition, our 1.43 GHz map has a much higher angular resolution. This enables us to conduct studies of the distribution of radio continuum emission, the radio spectral index, as well as synchrotron polarization and thereby the magnetic field of NGC 4666 with a spatial resolution of 1.8 kpc[1].

2. Observations and data reduction

We obtained a set of optical and radio data for NGC 4666 in several observing runs, using different telescopes. Some basic information on the observations is collected in Table 1. The individual datasets are described in more detail below. A 17 ksec integration with the ROSAT Position Sensitive Proportional Counter (PSPC) of the 0.1–2.0 keV soft X-ray emission of NGC 4666, which we obtained in addition, will only be mentioned briefly here and presented in detail in a different context (Dahlem et al., in prep.).

2.1. Optical imaging and spectroscopy

The optical spectroscopic and imaging data are taken from three separate observing runs. A complete discussion of the reduction and analysis of optical images, obtained with the CTIO 1.5-m telescope, and the red minor axis spectrum, using the Las Campanas 2.5-m telescope plus the modular spectrograph, can be found in Lehnert (1992).

2.1.1. Optical R-band and Hα imaging

Our optical imagery was in brief as follows. Both images, the R-band continuum and Hα+N [II], were processed in a standard fashion using the IRAF package produced by NOAO (Lehnert 1992), using dome flat field exposures to correct for inhomogeneities in the sensitivity of the CCD chip, and an average of many bias frames scaled by a fit to the overscan region to correct for the DC offset. The pixel size of the Tek 1024 chip corresponds to $0\farcs48^2$, providing a total field of view of $7\farcm4 \times 7\farcm4$. The seeing was about $1\farcs4$ (R-band) and $1\farcs9$ (Hα).

2.1.2. Optical spectroscopy

Our red spectrum of NGC 4666 was taken on the night of March 2, 1990 (UT) with the DuPont 2.5-m telescope on Las Campanas. We used the modular spectrograph with the 85 mm camera and a TI 800 CCD. The spectral resolution is about 4 Å, the spatial scale is $0\farcs85$ pixel^{-1}, and the projected slit width is $2\farcs5$. The slit was centered on the maximum of the optical red continuum emission, cutting through the galaxy along the minor axis at a position angle of $PA = 132°$. We integrated for a total of 1 hour. The final spectrum covers the spectral region of 5960 – 7180 Å, which includes the low-ionization lines of O [I]λ6300, N [II]λ6583, and the S [II]$\lambda\lambda$6716, 6731, as well as Hα.

A long-slit blue spectrum was taken during the night of March 23, 1993 (UT), using the CTIO 4-m telescope in combination with the Ritchy-Chrétien spectrograph. We used the KPGLF grating (632 l mm^{-1}) in second order and a Tek 1024 CCD. The resolution of the spectrum is 1.5 Å and it covers a wavelength range from 4340 to 5200 Å, including the Hγ, Hβ, and O [III]$\lambda\lambda$4363,4959, and 5007 Å emission lines. The slit width is 375 μm, or $2\farcs5$, and the usable slit length is nearly $5'$, with a scale along the slit of $0\farcs787$ pixel^{-1}. Again, the slit was oriented along $PA = 132°$, approximately the minor axis of NGC 4666, passing through the maximum of the optical continuum. Our final spectrum is a result of averaging three 1800 sec exposures. The data were flat-fielded, bias subtracted, and scaled by the mean of the CCD overscan region. Flux calibration was achieved using exposures of the stars LTT 2415, LTT 7393, and LTT 6248 taken with a $10''$ wide slit. We measured the fluxes, widths, and redshifts of the emission lines using the IRAF task SPLOT. The spectra were extracted and measured in sums of 3 CCD rows ($\approx 2\farcs4$) along the slit. Since the seeing was better than $2\farcs4$, each sum contains independent spatial information.

The blue spectrum of NGC 4666 was found to have a strong underlying stellar continuum over a region of about $25''$ on each side of the nucleus along the minor axis. Over this region, the

[1] Throughout this paper we will adopt a distance to NGC 4666 of 26.3 Mpc, based on $v_{\rm hel}$ = 1520 km s^{-1}, under the assumption of $H_\circ$ = 75 km s^{-1} Mpc^{-1}, and a virgocentric infall velocity of 300 km s^{-1}.

stellar continuum has a very strong Hβ absorption line which obviously affects the measured strength of the Hβ emission line. This effect tends to make the measured ratio O [III]λ5007/Hβ much higher than it really is (although the absorption line spectrum is strong enough to also affect the strength of O [III]λ5007 over this region as well). Since, as will be discussed later, our results depend sensitively on the O [III]λ5007/Hβ ratio in particular, we tried to subtract the stellar continuum from each of the spectra generated by summing CCD rows of the high-resolution long-slit spectrum.

To remove the rather strong Balmer absorption lines, we tested previously obtained high signal-to-noise (S/N) spectra of NGC 205, M 32 and the bulge of M 31 to determine which of them is the best template for removing the effects of the stellar population in the spectrum of NGC 4666. Each spectrum has 1.7 Å pixel^{-1} resolution and covers from 3520 to 5330 Å (Heckman 1978). After resampling and trimming them to match the dispersion and spectral coverage of our spectrum of NGC 4666, these spectra were then redshifted to match the redshift of the G-band and the Hβ absorption lines plainly visible in all of the spectra extracted near the nucleus. Since the stellar population of NGC 4666 is likely to dominate its continuum emission, we subtracted the continuum completely using the renormalized template spectra of NGC 205, M 31, or M 32 to determine which one gives the best representation of the continuum of NGC 4666. The spectrum of M 32 (which led to no gross distortions of the continuum, did not cause any unreasonably broad component of emission in Hβ to be seen, and did not leave the Hβ or nearby absorption lines incompletely "filled in") was judged the most appropriate. Therefore, all of the O [III]λ5007/Hβ ratios within 25″ on either side of the nucleus quoted in this paper are a result of a continuum subtraction using M 32 as a template for the absorption line spectrum. Note that this does *not* affect the data at minor axis offsets $> 25''$.

2.2. Radio continuum synthesis imaging

We observed NGC 4666 at two frequencies, 4.89 GHz and 1.43 GHz, with the VLA[2]. The observing dates and array configurations are compiled in Table 1. The data were reduced in the standard fashion using the NRAO AIPS package. 3C286 and 1246-075 were chosen as flux and phase calibrators, respectively. For 3C286 we calculated total flux values of 7.55 Jy (4.89 GHz) and 14.84 Jy (1.43 GHz). 3C286 was also used as polarization calibrator and therefore observed several times during the syntheses.

In the reduction of the 4.89 GHz observations the data for both observing days were calibrated separately, checked for consistency and then combined. The combined visibilities were Fourier-transformed onto a grid with 4″ pixel size, cleaned, and restored with a synthesized beam of $HPBW$ = 14″. In order to increase the dynamic range of the final images, the data were phase self-calibrated. The final noise level (rms) is 12 μJy beam^{-1} (dynamic range $\simeq$ 1000). Since the extent of NGC 4666 of 4′.7 (see below) is about half the primary beam width (PBW) of the VLA telescopes at 4.89 GHz (9′), all 4.89 GHz radio maps were primary-beam corrected, which is particularly important for quantitative statements on the spectral index (§§ 3.6 and 3.7) and the polarization degree (§ 3.8). The residual calibration uncertainties in the orientations of the E-vectors are $< 3°$, the uncertainty of the polarization degree is $< 0.5\%$. Before combining the Stokes Q and U data from both intermediate frequency channels (IFs), we made sure that the differences in Faraday rotation between the two bands are negligible.

The 1.43 GHz observations were processed in exactly the same fashion as the 4.89 GHz data, including phase self-calibration and polarization calibration. The $HPBW$ of the synthesized beam is again 14″. However, since the PBW is much broader at 1.43 GHz (30′) than at 4.89 GHz (9′), no correction for primary beam attenuation was necessary. The final noise level of the 1.43 GHz map is 40 μJy beam^{-1} (corresponding to a dynamic range of $\simeq$ 800). Residual phase errors limit the dynamic range of this map, while the 4.89 GHz image is noise limited. The lower quality of the 1.43 GHz map is the reason why we cannot make any statement on the spectral index distribution at faint levels (see below).

3. Results

3.1. Optical continuum image of NGC 4666

Fig. 1 shows our R-band image of NGC 4666, displayed on a logarithmic grey scale. The field of view extracted from the original frame is 5′.1 × 5′.4 (39.0 × 41.3 kpc). NGC 4666 has a prominent dust lane with interspersed bright emission from H II regions in the outer disk. The high inclination and the appearance of the dust lane make it clear that the south-east edge of NGC 4666 is pointed towards us and the north-west edge is on the far side of the galaxy. Together with the CO position-velocity (pv) diagram by Young et al. (1995) this determines the true sense of the galaxy's rotation.

3.2. The distribution of optical emission line gas

In Fig. 2 we display the Hα+N [II] narrow-band image of NGC 4666 from Lehnert (1992), using a double-logarithmic grey scale. Three features are visible in the data: 1) of order 100 luminous H II regions in the galaxy disk; 2) emission line filaments reaching out of the disk into the halo; 3) diffuse ionized gas (DIG) in the central region and in between the H II regions, and also in parts of the halo. The displayed field of view is identical to Fig. 1.

In the disk of NGC 4666 the number of luminous H II regions is high compared to many other galaxies. Kennicutt & Kent (1983) measured a median equivalent line width (EQW) of the Hα+N [II] emission lines of a large sample of galaxies, which for the Sc galaxy subsample is $\approx$ 25 Å. NGC 4666, with an EQW of 31 Å, is among the most actively star-forming galaxies of Hubble type Sc (see also Kennicutt et al. 1989). For comparison,

[2] The VLA is a facility of the National Radio Astronomy Observatory, which is operated by Associated Universities, Inc., under contract with the National Science Foundation

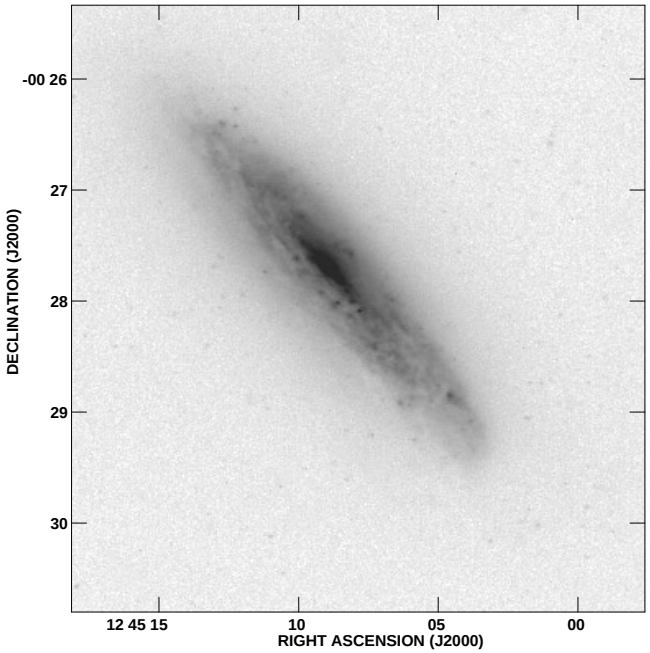

Fig. 1. Optical R-band image of NGC 4666. North is to the top, East to the left; the displayed field of view is $5\farcm1 \times 5\farcm4$ (39.0 kpc $\times$ 41.3 kpc).

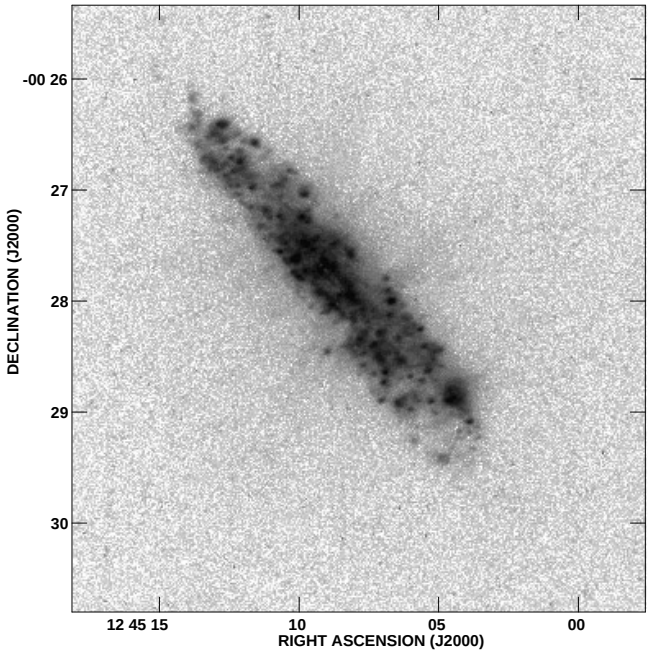

Fig. 2. Continuum-subtracted narrow-band Hα+N [II] image of NGC 4666. The orientation and the field of view are identical to Fig. 1.

NGC 4631 (Hubble type SB(s)d) has an EQW of 39 Å. From our own data we measure an even higher EQW for NGC 4666 of 44 Å. One of the brightest Hα+N [II] emitters in NGC 4666 is a giant extragalactic H II region (GEHR; Kennicutt 1984) about $1\farcm6$ south-west of the centre of NGC 4666, which will be discussed in more detail below. The half light radius of Hα emission is $27'' \pm 2\farcs5$ (3.5 ± 0.35 kpc).

In the halo the most extended optical emission line filaments, which form an "X"-shaped structure (cf. the plates in Lehnert & Heckman 1996), reach out to z-distances above the plane of up to $\approx$ 7.5 kpc at a surface brightness of $\approx 5 \times 10^{-17}$ ergs s^{-1} cm^{-2} arcsec^{-2}. Above the luminous GEHR south-west of the centre an emission line filament with a length of $\approx$ 2.4 kpc is visible, which appears to root in that H II region and thereby indicates that warm ionized gas exists in the halo of NGC 4666, with a direct connection to the activity in the underlying disk. Part of the line emission in the halo might be diffuse.

3.3. Excitation conditions of the emission line gas

The spatial information in the long-slit spectra allows us to determine the emission line properties as a function of height above the disk along the minor axis. There are pronounced spatial variations in the widths, velocities and emission line ratios along the minor axis of NGC 4666 (Figs. 3 and 4). The emission line ratios of O [I]λ6300/Hα, N [II]λ6583/Hα, S [II]$\lambda\lambda$6716, 6731/Hα, and O [III]λ5007/Hβ all increase with projected height above the mid-plane of NGC 4666. With the exception of O [I]/Hα, the run of emission line ratio with projected height for all these lines goes in approximately the same way. The line ratios have a maximum at the nucleus, minima in areas where the line of sight cuts through the disk with its H II regions ($\leq 20''$ from the major axis), rising rapidly again with increasing z-distance beyond the disk of NGC 4666. At z-distances of $40''$ to $60''$ (5 to 7.5 kpc) away from the major axis the ratios reach their maximal values. At the position of the nucleus the O [III]λ5007/Hβ line ratio is not well determined due to underlying absorption.

3.4. Kinematics of the emission line gas

The line widths and the recession velocities in the spectra also reveal interesting structure (Fig. 4). We measure a velocity gradient of the emission line gas of about 100 km s^{-1} over the $\pm$6.5 kpc range along the minor axis over which Hα and N [II] emission was detected. This is a clear kinematic signature of an outflow that is viewed close to (but not exactly) edge-on, as first found in M 82 by Lynds & Sandage (1963).

The line widths have a run of width versus height above the plane which is similar to the run of line ratios versus height above the plane (Fig. 3). That is, there are broad lines on the nucleus ($\sim$180 km s^{-1}), which then narrow over the next $10''$ to $20''$ (to $\sim$ 80 km s^{-1}), and subsequently broaden again, reaching a maximum $FWHM \approx$ 180 km s^{-1} at heights of about $40''$ (5 kpc). This plot shows that, based on emission line widths, the same three spatial regimes can be distinguished that were already identified through the observed line ratios: the nuclear region, the regime where the line of sight cuts through the disk, and the halo.

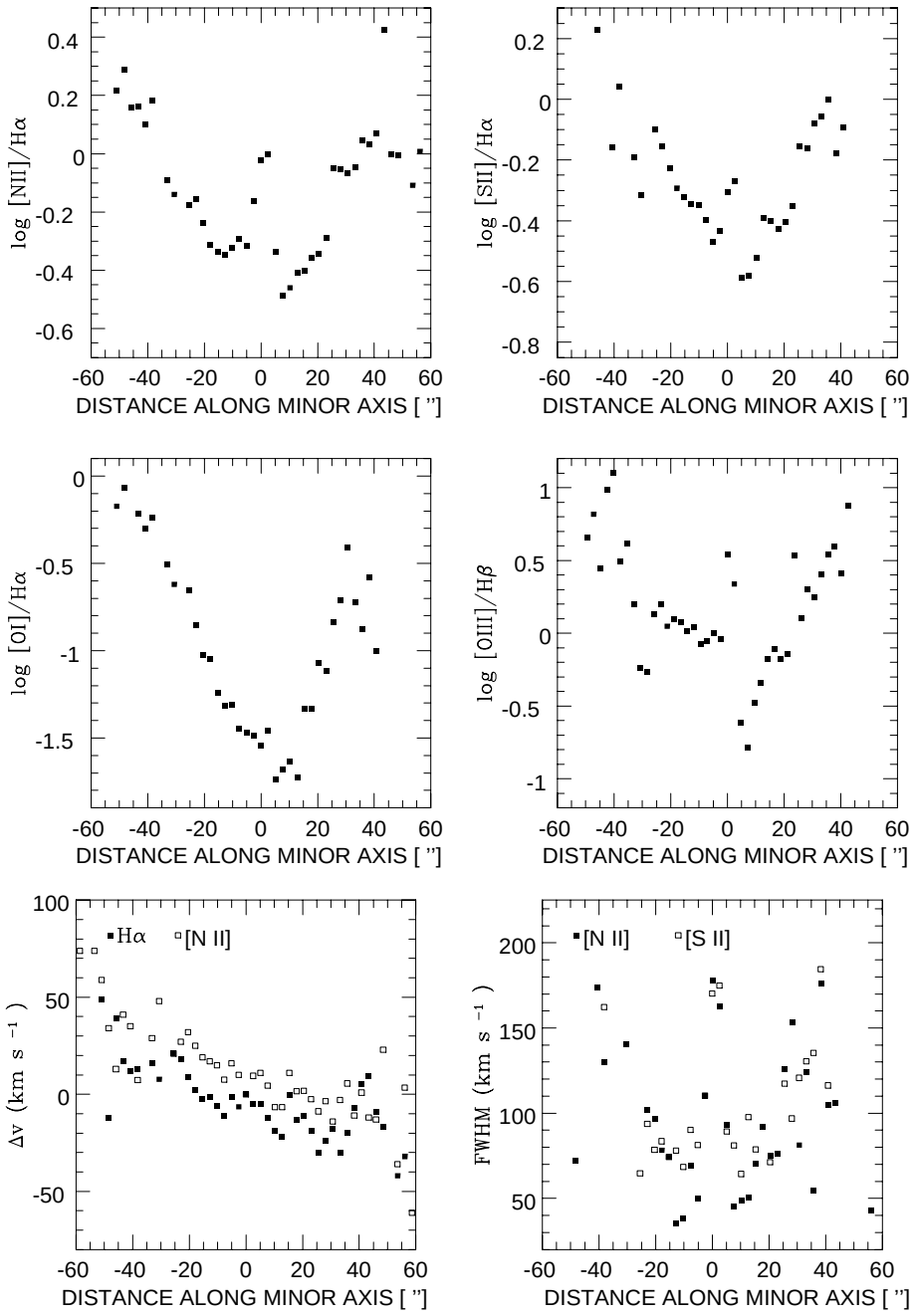

Fig. 3. The run of line ratios with projected distance above the plane of NGC 4666.

Fig. 4. The kinematics of the minor axis spectrum of NGC 4666. On the left we display the run of velocity relative to the nucleus versus the projected minor axis distance and on the right we plot the full width at half maximum of the N [II]λ6583 line and the S [II]$\lambda\lambda$6716, 6731 lines.

3.5. High-sensitivity radio maps of NGC 4666

Fig. 5 (left panel) shows a map of the total emission of NGC 4666 at 4.89 GHz. In the right panel we display the same field of view, now at 1.43 GHz. Both the resolution (14″) and the pixel size are identical, because we obtained the data with so-called "scaled arrays" of the VLA. In both images one can distinguish two components of radio continuum emission: a radio-bright thin disk and a halo of lower surface brightness.

Together with the total power information we show polarization E-vectors in both maps. This will be described in § 3.8. Most of the polarized emission at both observing frequencies arises from areas close to the major axis. The highest polarization percentages (depicted by the length of the vectors) is observed in the halo of NGC 4666.

From both maps we can measure the position of the galaxy centre to be $\alpha, \delta(2000) = 12^{\rm h}\,45^{\rm m}\,08\overset{\rm s}{.}62 \pm 0\overset{\rm s}{.}03, -00^\circ\,27'\,44\overset{''}{.}9 \pm 0\overset{''}{.}5$. The PA of NGC 4666, measured from both radio maps, is $221^\circ \pm 1^\circ$.

3.5.1. Radio continuum emission from the thin disk

The radial extent at the 1%−level of the radio synchrotron emission along the major axis is 4′.7 (36 kpc). Along the major axis the synchrotron emission has a spatially resolved broad maximum in the central part of the disk, with a half light radius of

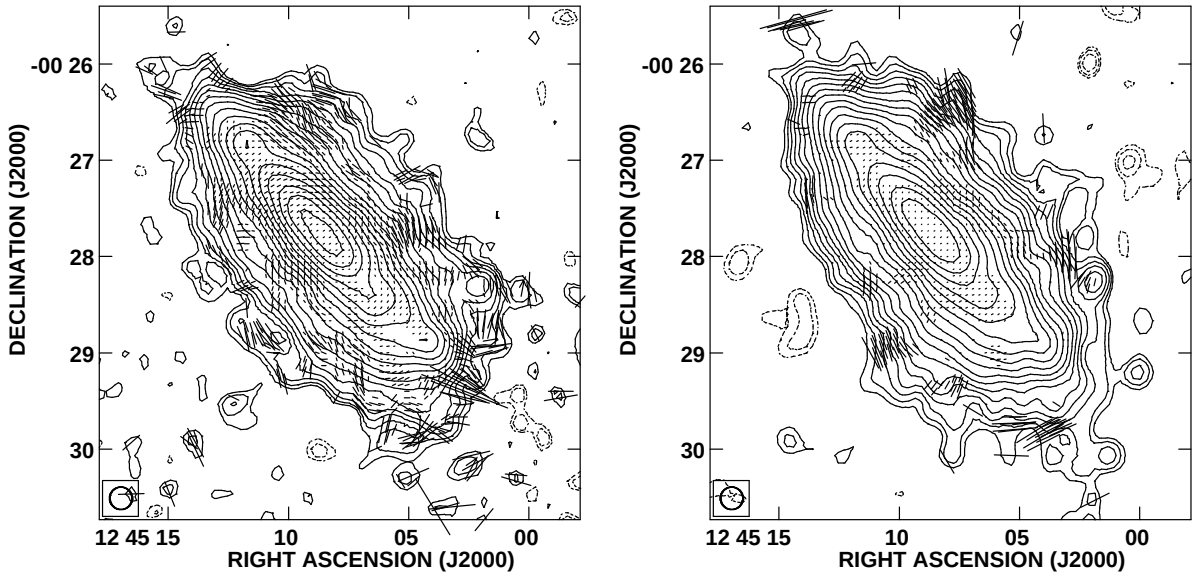

Fig. 5. Left panel: contour map of the 4.89 GHz emission, with E-vectors superimposed at positions where the polarization percentage, $P_{\%}$, exceeds 1%; right panel: the same at 1.43 GHz; the length of the polarization vectors is proportional to $P_{\%}$. E-vectors are shown only in areas where both the total and the polarized flux densities are above the $2-\sigma$ significance level.

$25'' \pm 1\farcs5$ (3.2 ± 0.2 kpc). There is no high-brightness compact core which might indicate the presence of an AGN. Instead, the bright emission must arise from SF regions close to the centre. In the outer disk the surface brightness is considerably lower (about $15-30\%$ of the maximum). Three secondary maxima are visible, two south-west of the centre, one north-east of it. The maximum $1\farcm6$ south-west of the centre is the bright GEHR in Fig. 2 (§ 3.2).

3.5.2. The synchrotron radio halo of NGC 4666

The disk of NGC 4666 is not perfectly edge-on and thus appears to be broader than the resolution of our data. Fig. 5 shows that the radio emission extends about $\pm 60''$ (± 7.5 kpc) from the major axis at the 1%-level of the peak flux. In order to determine whether this broad emission distribution might be caused by a thin, but somewhat inclined disk or whether a second component – namely a radio halo – exists, we produced profiles perpendicular to the major axis. The data for $|z| \leq 40''$ are shown on a logarithmic scale in Fig. 6. The cuts represent the mean emission distribution along the minor axis, averaged in the major axis direction over a range -10.3 kpc $\leq r \leq +10.3$ kpc, centred on the nucleus of NGC 4666, thus excluding the point source to the west of the galaxy. In the minor axis (z-)direction the cuts span a range of ± 5 kpc.

Due to its inclination of about 80° (RC3), the disk of NGC 4666 appears to be broader than the beam in Fig. 6. Using only data points above 20% of the maximum, we find a best Gaussian fit to the data (both 1.43 and 4.89 GHz) with a $FWHM$ of $25\farcs9 \pm 2\farcs0$. Approximating the disk emission profile by a simple box function (constant within a given range and 0 outside), and formally deconvolving by the $14''$ Gaussian beam, we find an equivalent width of the thin radio continuum disk of $21\farcs7 \pm 2\farcs0$. Adopting that the disk is infinitely thin, this leads to an inclination angle of about $85° \pm 3°$, which is – within the uncertainties of the measurements – compatible with the optical value of 80°. The fitted disk profile is shown as a dotted line. Close to the disk plane this model is obviously a very good approximation to the data. However, the extended wings of the emission distribution at $|z| > 20''$ cannot be fitted. This means that a second emission component, a radio halo, does indeed exist. The wings decrease exponentially with increasing distance from the major axis, which is typical of radio synchrotron halos (e.g. Hummel & Dettmar 1990; Dahlem et al. 1994). Excluding now the disk emission (using only data points at $\pm 40'' \geq |z| > \pm 20''$) and averaging the values from both sides of the halo, we calculate the exponential scale heights of the halo emission at 4.89 GHz of $z_0 = 12\farcs1 \pm 2\farcs3$ (i.e. 1.54 ± 0.29 kpc) and at 1.43 GHz of $z_0 = 13\farcs3 \pm 2\farcs2$ (1.70 ± 0.28 kpc). A comparison with observations of NGC 891 and NGC 4631 reveals that the average scale height of the radio halo in NGC 4666 lies in between those of the former (see Table 2).

Table 2. Scale heights of galactic radio halos at 1.49 GHz

Galaxy	z_0 ($''$)	z_0 (kpc)	D (Mpc)
NGC 891[1]	26.5	1.2	9.5
NGC 4631[2]	59.7	2.2	7.5
NGC 4666[3]	13.3	1.7	26.3

Notes to Table 2:
[1] Dahlem et al. (1994)
[2] Hummel & Dettmar (1990)
[3] This paper.

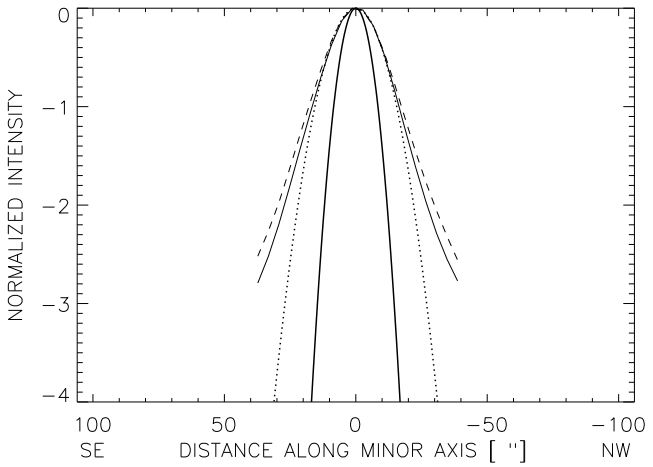

Fig. 6. Cuts through the radio maps of NGC 4666 along the minor axis (PA = 131°). The width (parallel to the major axis) of the cuts is 40 pixels (160″), the length along the minor axis is 80″ (±5 kpc from the disk plane). 4.89 GHz data (solid line), 1.43 GHz (dashed line), and the beam (bold line) are displayed. The dotted line illustrates the instrumental profile for an infinitesimally thin disk inclined at an angle of 85°.

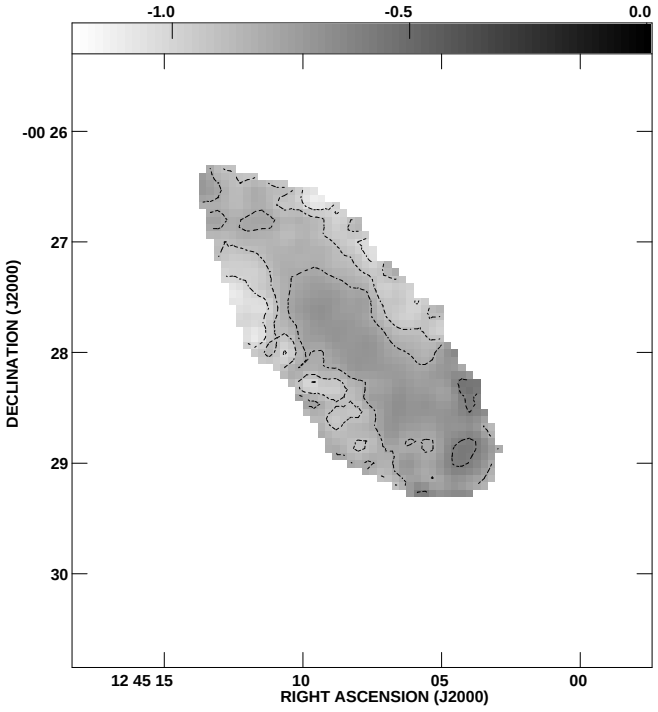

Fig. 7. Radio spectral index ($\alpha_{4.89}^{1.43}$) map of NGC 4666 from the two continuum images in Fig. 5. The resolution ($HPBW$) is again 14″. The grey scale ranges from –1.2 (white) to 0 (dark grey), see wedge. Pixels with undefined values are blank.

Within the halo one elongated feature (which we will call a "spur") of radio emission is discernible almost exactly 40″ west of the centre. In the contour representation of both maps in Fig. 5 it shows up as an outward bending of all contours up to very high levels of surface brightness. This spur foots in a part of the disk where the highest number of H II regions is seen in Hα, thereby suggesting a connection between disk activity and halo properties.

3.6. Radio total flux measurements and integral spectral index

From our 4.89 GHz map we calculate a total flux of NGC 4666 of 155 ± 7 mJy. The contribution of the weak point source at $\alpha, \delta(2000) = 12^{\rm h}\ 45^{\rm m}\ 02\overset{\rm s}{.}26, -00°\ 28'\ 18\overset{''}{.}9 \pm 0\overset{''}{.}5$, west of the galaxy disk is insignificant ($\simeq$ 0.4 mJy), but was taken into account. With a shortest spacing of 35 m (0.58 kλ) we can be sure that the full flux was observed and the above measurement of 155 mJy is in agreement with the value of $S_{4.75GHz}$ = 157.3 ± 4.3 mJy obtained by SVK with the Effelsberg 100-m single dish.

Using the same region for the total flux measurement as for the 4.89 GHz data, we measure a total 1.43 GHz flux of NGC 4666 of 408 ± 20 mJy. SVK measured the total radio continuum flux of NGC 4666 at three frequencies, 0.33 GHz, 1.47 GHz, and 4.75 GHz. Our 4.89 GHz flux measurement is in agreement with their value. At 1.43 GHz, however, we find a slightly higher flux than SVK (who obtained 376.3 ± 18.8 mJy), probably because our map is much more sensitive so that we are picking up more extended emission from the outer parts of the halo. Thus, the integral spectral index following from our data of $\bar{\alpha}_{4.89}^{1.43}$ = −0.79 ± 0.06 is marginally steeper than, but still compatible with, the value published by SVK (–0.76). These values of $\bar{\alpha}$ are very close to the average spectral index derived for a large sample of 56 spiral galaxies by Gioia, Gregorini, & Klein (1982), of $\bar{\alpha}$ = −0.74.

3.7. The spatial radio spectral index distribution

The two total power maps presented above can be used to study spatial variations of the radio spectral index along the disk of NGC 4666 and perpendicular to it. In Fig. 7 we show our map of the spectral index $\alpha_{4.89}^{1.43}$. α is given only for regions where the 1.43 (4.89) GHz emission is above 0.6 (0.3) mJy beam^{-1}. Along the major axis α is surprisingly constant compared to NGC 891 and NGC 4631 and it is also lower than in these two galaxies (see Hummel et al. 1991). The spectrum is flattest (–0.7) in the central 1′, dropping slightly with increasing galactocentric distance to values close to –0.9. One feature sticks out clearly: a local maximum of α about 1′.6 south-west of the galaxy centre. This is the location of the bright GEHR which will be discussed in more detail in § 4.3. Elsewhere in the disk several other groups of H II regions are marginally discernible by their relatively flat radio spectra. Perpendicular to the disk of NGC 4666 the spectral index steepens slightly, to a minimum of about –1.0. The spectral steepening away from the disk plane is consistent with the different scale heights measured at 1.43 GHz and 4.89 GHz (above).

3.8. Polarized radio emission

In Fig. 5 we present, together with the total intensity distribution of NGC 4666, E-vectors at 4.89 and 1.43 GHz. The detected extended polarized emission proves that large-scale ordered magnetic fields exist in NGC 4666. The resolution of our data is about 2 kpc at its distance, implying that the physical scales of the detected ordered B-field structures are larger than 2 kpc. Most of the polarized emission at both observing frequencies arises from areas close to the major axis. The highest polarization percentages (depicted by the length of the vectors) are observed in the halo of NGC 4666.

Hummel et al. (1991) noted that the polarization degree increases as a function of the distance from the major axes of NGC 4631 and NGC 891. The same is observed in NGC 4666. At $|z| > 30''$ (3.8 kpc) from the major axis, $P_{\%}$ rises to values of 5 to 30%. In the disk, i.e. close to the major axis, $P_{\%} \lesssim 5\%$ in NGC 4666. Due to the non-detection of polarized emission in some regions, the emission distribution looks somewhat "patchy". However, the orientation of the E-vectors shows a smooth distribution with no obvious indications of any possible field reversals.

4. Discussion

4.1. The distribution of star-forming regions and the level of star formation in the disk of NGC 4666

Following Devereux & Young (1991), the FIR luminosity given above corresponds to a mean star formation rate (SFR) of massive stars in NGC 4666 of 7.0 $M_{\odot}$ yr^{-1}. Both our optical and radio data show two major areas in NGC 4666 in which SF is going on at a high level: an extended central starburst and a large number of luminous H II regions in the outer disk.

The central starburst has a diameter of about 6.5 kpc, which can be measured from both the locations of some of the most prominent H II regions in Fig. 2 and the radial extent of the central radio continuum emission maximum. This starburst extends approximately to the turnover of galactic rotation, where the largest concentration of molecular gas is found (see CO measurements by Young et al. 1995).

In the outer disk, beyond the central starburst, H II regions and radio continuum emission are detected out to a maximal galactocentric radius of about 16 kpc. The surface brightness of the radio continuum emission in the outer disk is at a level of $15-30\%$ of the central peak, but the level of SF – as also traced by the bright Hα emission – is still high.

All these properties make NGC 4666 very similar to NGC 4631 (Golla & Hummel 1994; Golla & Kronberg; in prep.). One more similarity between NGC 4666 and NGC 4631 is that both lack any strong central concentration of molecular gas (Golla & Wielebinski 1994; Young et al. 1995) and have shallow velocity gradients over the central few kpc. All of these similarities of the two galaxies lead us to the prediction that very sensitive high-resolution radio maps will reveal the presence of a population of compact radio sources (SNe, young SNRs, and primarily the optically visible H II regions) in the disk of NGC 4666, as found in NGC 4631 by Golla & Kronberg (in prep.).

The measured radio spectral indices give a hint at the locations of the highest level of SF: the flat spectrum especially of the GEHR south-west of the centre indicates a high fraction of thermal emission (with $\alpha = -0.1$).

4.2. Optical line and radio continuum emission from the halo

4.2.1. The central outflow cone

Our Hα+N [II] image suggests that the central starburst in NGC 4666 is associated with a classical outflow cone. Because of the multitude of bright Hα-emitting SF complexes seen in projection near the nuclear region, the walls of the cone cannot be traced close to the disk plane, but only out in the halo (especially on the north-west side, at projected distances of > 2.5 kpc from the centre; $> 20''$ from the major axis). Although their surface brightnesses are very low (down to 5×10^{-17} ergs s^{-1} cm^{-2} arcsec^{-2}), Fig. 2 shows filaments extending out to about 5.5 to 7.5 kpc. Extrapolating their orientations into the disk plane, one can see that they do not appear to foot in the galaxy centre, but rather in the H II regions at the outer edges of the central starburst.

Based on morphological information, i.e. the extent of the central starburst and the orientation of the most prominent Hα filaments, the following (axisymmetric) geometry describes the shape of the outflow quite well: a base in the disk of the galaxy of diameter 6.5 kpc (i.e. the half light diameter of the Hα and radio continuum emission) and an opening angle of $30^{\circ} \pm 10^{\circ}$ (following the most prominent Hα filaments and the radio continuum spur). This scenario is sketched in Fig. 2. The cone encompasses the soft X-ray emission displayed in Fig. 8 (see below).

The velocity gradient found along the minor axis (Fig. 4) is an additional indication of an outflow. However, it cannot be used to further constrain the kinematic parameters of the outflow unless the radial expansion velocity of the cone is measured in the plane of the galaxy, as done for M 82 by Götz et al. (1990).

The Hα emission on the south-east side of the cone is weaker than in the north-west due to obscuration by the front side of the thin disk of NGC 4666 (Dahlem et al.; in prep.).

4.2.2. Hot gas in the central cone

In our ROSAT pointing (Dahlem et al.; in prep.) we clearly detect extended soft X-ray emission from the halo of NGC 4666 in the softest part of the ROSAT passband, the so-called 0.25 keV band (Snowden et al. 1994), see Fig. 8. Although the S/N in this image is low, one can clearly see that the emission is centred away from the disk plane of NGC 4666. The single-sided appearance is due to absorption of soft X-ray emission from the backside (the south-east side) in H I gas in the disk. This effect is discernible when comparing the 0.25 keV image with the higher energy bands (not displayed), which show a less asymmetric emission distribution. A more detailed picture will arise from future VLA H I line observations. All this is consistent with the above results of our Hα imagery. The 0.25 keV emission

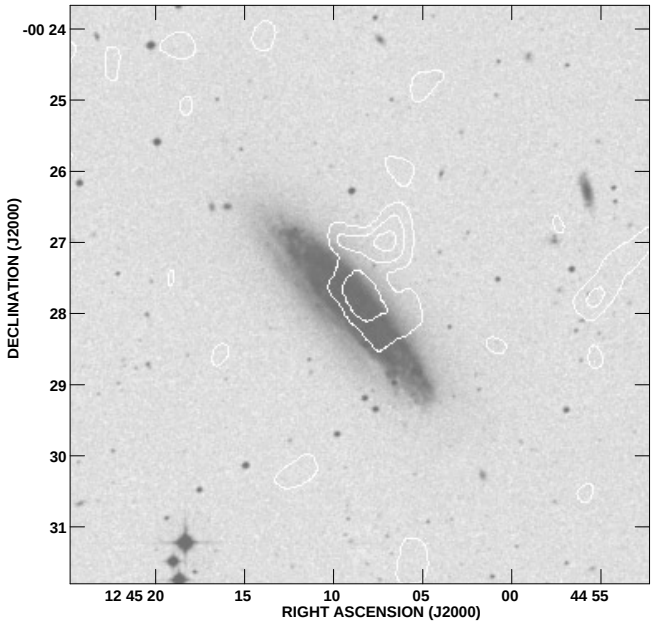

Fig. 8. ROSAT PSPC image of NGC 4666 at an energy of kT = 0.25 keV, superimposed on a digitized sky survey image. The field of view is $8' \times 8'$. The contours represent the $2-\sigma$, $2.8-\sigma$, and $4-\sigma$ significance levels (from Dahlem et al.; in prep.).

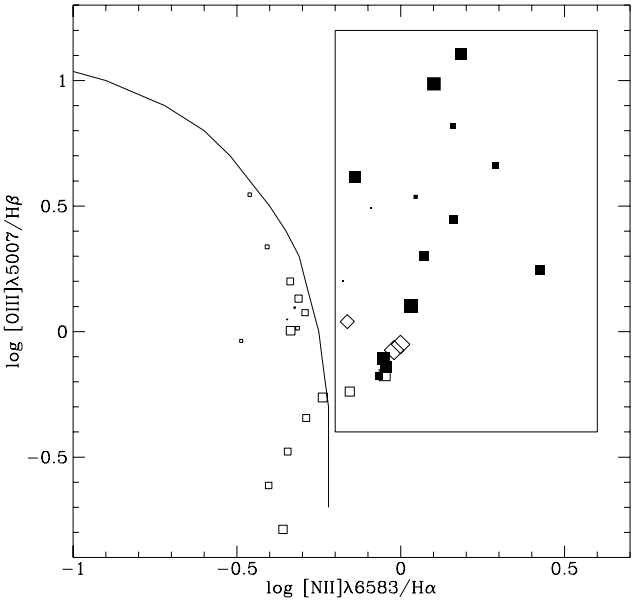

Fig. 9. Emission line diagnostics for points measured along the minor axis of NGC 4666, according to Osterbrock (1989). Data points from the nuclear region are shown as open diamonds, open squares represent measurements in the thin disk, and filled squares depict line ratios observed in the halo of NGC 4666. The symbol sizes are proportional to the observed N [II] line width at each given point.

is located between the most prominent Hα filaments which very likely form the outer rims of the outflow cone. In this scenario, the soft X-ray emission traces hot gas within the outflow, with a temperature of $2 - 3 \cdot 10^6$ K. The softness of the emission is consistent with shock heating of the gas (Suchkov et al. 1994).

4.2.3. The ionization source of the emission-line gas

Our optical spectroscopic results suggest that we are viewing three different physical gas components along the minor axis of NGC 4666: the nuclear region, then cutting through the highly inclined thin disk, and further out pure halo emission. Fig. 3 illustrates this.

To learn more about the physical processes giving rise to the observed emission lines, it is useful to plot them in a diagnostic plot, as done by Osterbrock (1989). In Fig. 9 we show the ratio of log(N [II]/Hα) vs. log(O [III]/Hβ) for points measured along the minor axis of NGC 4666. Different symbols represent the various physically distinct components of the galaxy: open diamonds show the three points on the nucleus, open squares are points measured in the highly inclined disk ($|z| \leq 20''$), and filled squares represent data points at offsets from the major axis of $|z| > 20''$, where pure halo emission is seen. The curved line marks the empirical H II region fit by Baldwin et al. (1981). The rectangular box limits the expected range of emission line ratios of active galactic nuclei (AGN; Osterbrock 1989). The symbol sizes are proportional to the N [II] line width at each position. The plot confirms that the data points which we already tentatively associated with H II regions (above), do indeed exhibit the characteristic signatures, both in terms of line ratios and relatively low line widths. The nuclear data points fall into the area typical of low-ionization nuclear emission-line regions (LINERs; Heckman et al. 1983) and their line widths are accordingly higher than those of the H II region emission.

The most striking result is that the halo emission is clearly distinct from H II regions in the disk, with much larger line ratios and mostly higher line widths compared to the latter. An issue of particular interest is the heating source(s) of this extended gas. There are a number of viable theories for heating and ionizing it. As discussed by Lehnert & Heckman (1996), the most obvious possibilities are: 1) shock heating by an outflowing superwind (Heckman et al. 1993), 2) photoionization by the ionizing radiation field of the starburst that has been hardened by its passage through a neutral column of gas (Sokolowski 1995), and/or 3) by the development of turbulent mixing layers (Begelman & Fabian 1990).

Ad 1): Comparing the line ratios observed in NGC 4666 with shock models of Hartigan et al. (1987), Shull & McKee (1979), and Binette et al. (1985), we find that shock models are a reasonable match to the line ratios observed in the very extended emission line gas. For example, a shock with a velocity of 116 km s^{-1} and a pre-shock density of 10 cm^{-3} in the models of Binette et al. (1985) gives ratios of O [III]λ5007/Hβ = 5.4, O [I]λ6300/Hα = 0.2, N [II]/Hα = 0.8 and S [II]/Hα = 1.2; a shock with a velocity of 268 km s^{-1} and a pre-shock density of 10 cm^{-3} produces line ratios of O [III]λ5007/Hβ = 0.5, O [I]λ6300/Hα = 1.1, N [II]/Hα = 1.2, and S [II]/Hα = 2.6. The other models cited above lead to similar results. The observed values over 5 to 7.5 kpc from the mid-point of the

plane of NGC 4666 are roughly O [III]λ5007/Hβ = 1 to 10, O [I]λ6300/Hα = 0.1 to 0.8, N [II]/Hα = 0.6 to 2, and S [II]/Hα = 0.5 to 1.5. The match of the measured extended emission line ratios to those of shock models with shock speeds of one to several hundred km s^{-1} is generally quite good. Shock speeds this high are suggested by the soft X-ray emission and by the emission line widths and kinematics observed here (see §§ 3.3, 3.4, and 4.2.2).

Ad 2): What about the stellar population of NGC 4666 – could stars provide the ionizing energy of the extended emission line gas? For any reasonable choice of initial mass function and age of the starburst (10^{7-8} yrs), about 3 – 30% of the total bolometric luminosity of the starburst comes out as ionizing photons (e.g. Leitherer & Heckman 1995). Therefore, stars must play a role in the ionization of the emission line gas, at least in the disk of NGC 4666. However, the extended emission line gas in NGC 4666 does not appear to be simply photoionized by stars (i.e., it does not have exactly the same line ratios as H II regions). It may be possible to make the relative line ratios more similar to what is observed via photoionization if we allow the ionizing radiation to pass through a neutral column of gas, or allow for the depletion of metals on grains (Sokolowski 1995; see also Shields & Kennicutt 1995). Both approaches have been taken by Sokolowski (1995). Sokolowski found that both these mechanisms do indeed have the effect of increasing the ratios of N [II], S [II], and O [I] relative to Hα over ionization associated with the stars themselves (without altering the emitted stellar radiation field). Therefore, we have used his radiation bounded models with stellar radiation that has passed through a column of neutral material, resulting in an optical depth $\tau \approx 1$ at the Lyman edge with which to compare our results. We find that using these models, there is no way to reconcile all the line ratios measured here, using a single ionization parameter. For example, to explain the most extreme low-ionization (N [II], O [I], and S [II]) line strengths relative to Hα, an ionization parameter of about 10^{-5} to few times 10^{-3} is required. However, such a dilute radiation field predicts O [III]λ5007/H$\beta \ll 1$. We observe O [III]λ5007/H$\beta > 1$ in the most extended emission line gas. Therefore, we conclude that the diffuse ionizing radiation field of the starburst is not contributing significantly to the emission line properties of the most extended emission line gas.

Ad 3): Shock heating is not the only mechanism that could result in an emission line spectrum similar to the one observed in NGC 4666. Another possible mechanism are turbulent mixing layers (Slavin, Shull, & Begelman 1993), which arise when hot gas flows past a sheet of cold or warm gas. According to this hypothesis, the shear flow will excite Kelvin-Helmholtz instabilities at the interface between the two media, which grow until a layer of turbulent mixing exists over the interface region. The mixing gas then cools dissipatively, and possibly also through thermal conduction, passing through a stage in which it has a temperature between that of the warm and hot phase (at approximately the geometric mean of the hot and warm phases). Although there should be a range of temperatures in the turbulent mixing layer, at temperatures of about few $\times$ 10^5 K, the line emission from the mixing layer will be most intense in the UV and optical range. In the regions of contact along the walls of the ruptured bubble, hot gas ($T \sim 10^{6.5}$ K) is flowing past the swept-up, warm ($T \sim 10^4$ K) ambient ISM. The line ratios from Slavin et al. (1993) for turbulent mixing layers are in the range (for a turbulent velocity of 100 km s^{-1} and a temperature range of log T = 5.0 to 5.5) of O [III]λ5007/Hβ = 0.03 to 13.5, O [I]λ6300/H$\alpha \approx$ 0.03, N [II]/Hα = 0.2 to 0.7, and S [II]/Hα = 0.2 to 0.7. In general, the line ratios for turbulent mixing layers match the observed ranges of O [III]/Hβ, but they do not generally match those of the lower ionization ratios, especially O [I]λ6300/Hα. Specifically, we find that turbulent mixing layers predict O [I]/Hα that is too weak by an order of magnitude (O [I]/H$\alpha \approx$ a few hundredths compared to many tenths for NGC 4666; see Fig. 3).

Based on these results, the notion that either photoionization or turbulent mixing layers dominate the heating of the optical emission line gas can be dismissed. Considering the detection of hot ionized gas in the outflow cone, which is consistent with theoretical models of superwinds of galaxies (Suchkov et al. 1994), our data suggest the presence of a galactic superwind in NGC 4666, with shocks as the main sources of heating. Additional heating sources may exist and contribute significantly to the total energy balance, however they are not required to explain our observations. A confirmation of this interpretation comes from the similar runs of line widths and line ratios as functions of $|z|$, as described above (see § 3.4). This result suggests a direct relation between the gas dynamics and its excitation conditions (thus favouring an interpretation in terms of collisional excitation mechanisms over photoionization processes).

4.3. The large-scale gaseous halo

In addition to the cone of the central superwind, more diffuse Hα emission was detected in the halo of NGC 4666, at larger galactocentric distances. The most conspicuous Hα filament far away from the nuclear area is found above the very bright GEHR south-west of the centre (see Fig. 2). This filament, with a length of about 2.4 kpc, is an indication of an ongoing disk-halo interaction, initiated by the *local* energy input into the ISM by massive SF. A corresponding contour bending, tracing excess emission compared to the local surroundings, is visible in both radio maps (Fig. 5), although somewhat disturbed by the nearby background point source.

A quantitative determination of the difference in the radial extent of the synchrotron halo compared to the thin disk (as done by DLG95 for NGC 891 and NGC 4631) could not be carried out, mainly because of the non-perfect edge-on view of NGC 4666. Nevertheless, it is quite obvious from Fig. 5 that the total radial extent of the radio halo (parallel to the major axis of NGC 4666) is too broad to be explained by only an outflow cone above the central starburst. Part of the halo emission arises from the numerous luminous H II regions in the outer disk, as suggested by the outward bending of radio contours in particular above the prominent GEHR and in the region 1′ north of the nuclear region. In our Hα+N [II] image this region also exhibits faint diffuse optical line emission. Just like the radio

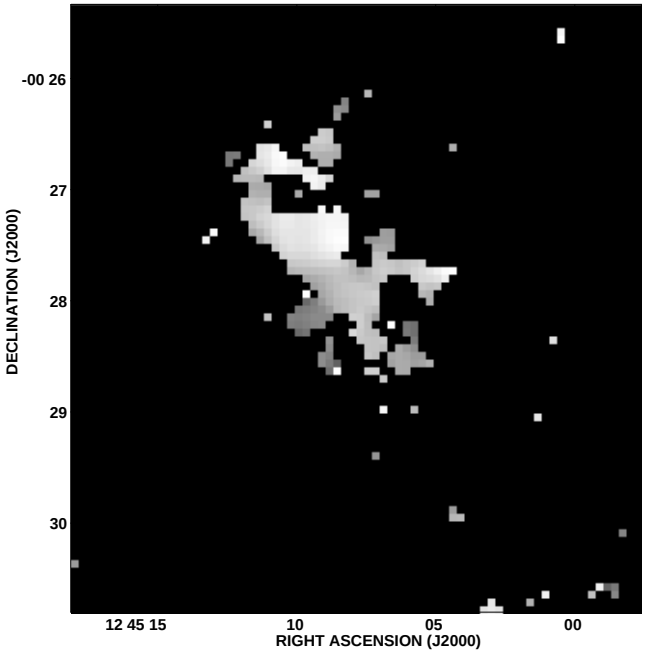

Fig. 10. Map of the distribution of rotation measures (RM) across NGC 4666 derived from the angles of the E-vectors shown in both maps in Fig. 5. The grey scale ranges from –39 rad m^{-2} (white) to +39 rad m^{-2} (dark grey). Pixels with undefined values are black.

emission, the Hα+N [II] line radiation does *not* look filamentary in this area, but diffuse. This corresponds most likely to the so-called "extraplanar diffuse ionized gas" (eDIG) detected in other galaxies, like e.g. NGC 891 (Dettmar 1990; Rand et al. 1990).

Another indication of disk-halo interactions outside the nuclear outflow cone is the general steepening of the radio spectral index away from the disk plane of NGC 4666 in Fig. 7. Since the spectral steepening is a sign of synchrotron and inverse Compton losses of the CRs (Berezinsky et al. 1990), outflows have to be occurring in the outer parts of the disk, at large galactocentric radii. The scale height of the radio halo in NGC 4666 is in between those of NGC 4631 and NGC 891 (Tab. 2), most likely due to different levels of SF in the disks of the three galaxies (see DLG95). However, no soft X-ray emission was detected outside the central outflow cone of NGC 4666. Although this might be due to sensitivity effects, it does indicate that the surface brightness of hot gas outside the superwind, if existent, has to be considerably lower than inside it. This is consistent with a lower SFR in the outer parts of the disk and consequently lower energy input rates and lower mass flow rates into the halo from the underlying disk (DLG95).

4.4. The orientation of the B-field in NGC 4666

In order to account for foreground Faraday rotation in the Galaxy (which is to first order a constant offset), we use rotation measure (RM) data of sources seen in projection close to NGC 4666. Based on a list provided by P. Kronberg (priv. comm.; Table 3) we calculate a mean foreground RM along the line of sight to NGC 4666 of $RM_{\rm Gal}$ = 6.4 ± 4.6 rad m^{-2}. This low foreground RM leads to rotations of the observed E-vectors of 16.°1(1.°1) at 1.43 (4.89) GHz. The external rotation, although almost negligible at 4.89 GHz, was taken into account when deriving the true direction of the magnetic field in NGC 4666. The low foreground RM is consistent with the high galactic latitude of NGC 4666 ($b_{\rm II}$ = 62.°4).

Table 3. Foreground rotation measure towards NGC 4666[1]

PKS Source	$l_{\rm II}, b_{\rm II}$ (°)	RM (rad m^{-2}) (rad m^{-2})	$\Delta\Phi$ [2] (°)
1237-101	298.2, 52.4	12	10.1
1239-04	298.64, 58.02	–10	4.5
1250-10	303.6, 52.4	6.8	10.8
1253-055	305.1, 57.1	15	7.7
1254-102	305.2, 52.39	8	11.5

Notes to Table 3:
[1] Kronberg (1995; priv. comm.)
[2] projected distance from NGC 4666.

In order to correct for the rotation of E-vectors of polarized synchrotron emission in interstellar matter along the line of sight to the observed object, one normally needs at least three observing frequencies. Observations at two frequencies are needed to derive the relative orientation of E-vectors within ±180°, while with data at a third freqency one can eliminate the remaining $\pm n \times 180°$ ambiguity. In the case of NGC 4666, the distribution of measured RMs (see below) is "good-natured", i.e. no 180° jumps are visible. Therefore, two observing frequencies are sufficient to map the magnetic field configuration. Combining the observations of the polarization angles at the two different wavelengths allows us to calculate the rotation measure, $RM = (\chi_2 - \chi_1)/(\lambda_2^2 - \lambda_1^2) \simeq 0.81 \int_0^L n_{\rm e}(s)\, B_{\parallel}(s)\, ds$, where $n_{\rm e}$ is the electron density of the gas in cm^{-3}, $B_{\parallel}$ the component of the uniform magnetic field parallel to the line of sight in μG, and the integration is along the line of sight of length L in pc. Using the observed polarization angles at both frequencies, we performed an RM analysis, utilizing the NOD2 package of MPI für Radioastronomie Bonn (Haslam 1974).

The resulting RM map of NGC 4666 is shown in Fig. 10. The RM values range from about −39 to +39 rad m^{-2} (the ambiguity being 78 rad m^{-2}), which leads to rotations of the E-vectors (and the orthogonal B-vectors) of up to ±10° at 4.89 GHz. By applying the calculated corrections and rotating the E-vectors by 90°, we derive the true orientation of the B-field vectors in NGC 4666. In Fig. 11 we display the 4.89 GHz radio map, now with the true B-vectors, overlaid on the Hα image in Fig. 2. Three nearby stars, just outside the plotted field of view, were used to align both images. The residual relative positional uncertainty is of the order of ±2″.

NGC 4666 exhibits a striking magnetic field geometry. While in the disk plane ($|z| < 15''$, or 2 kpc) the B-field vectors are consistent with a plane-parallel field, practically *all* B-vectors at high $|z|$ (> 2 kpc; i.e. beyond the point where we are

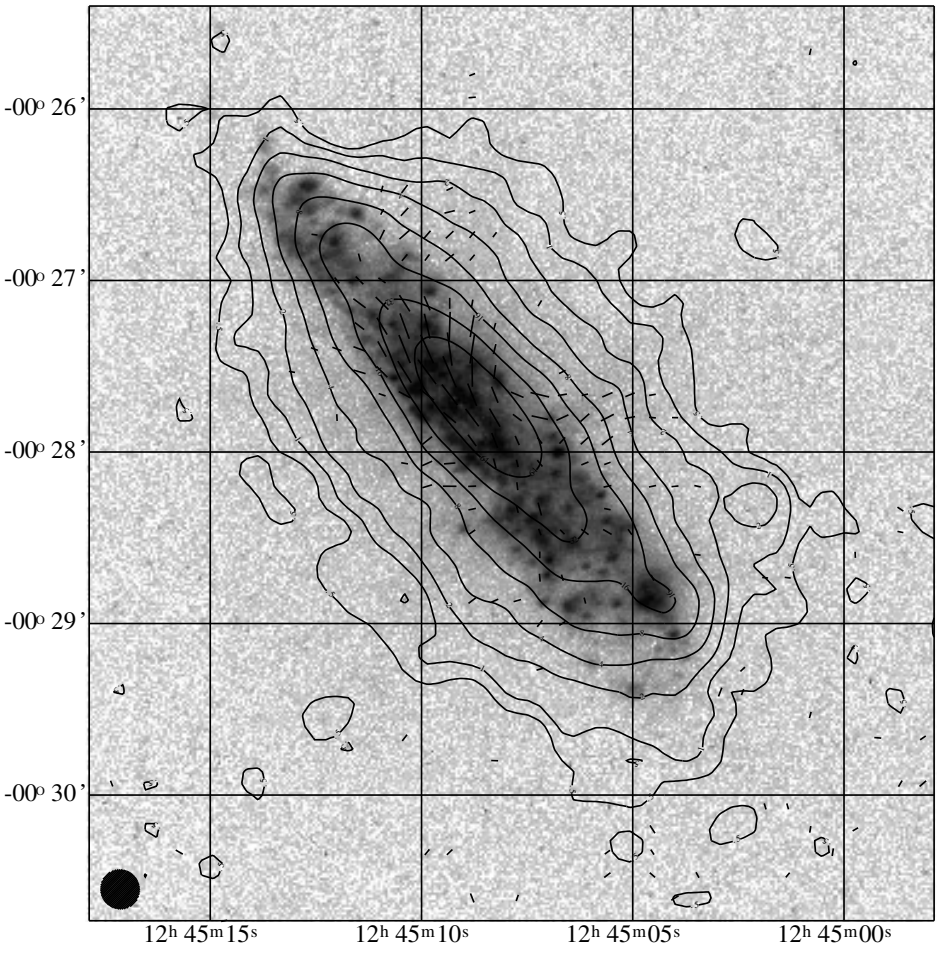

Fig. 11. Overlay of the magnetic field vectors on top of the Hα+N [II] image (Fig. 2), showing the spatial correlation of optical emission line and (polarized) radio synchrotron emission from the halo.

viewing the highly inclined disk in projection onto the minor axis) point away from the disk plane. This indicates magnetic field lines opening into the halo. Based on the assumption that, similar to M 82 (e.g. Völk et al. 1989), the CRs forming the radio halo originate in the disk of NGC 4666 we thus find morphological evidence for ongoing outflows of CRs along these open field lines: on the north-western side of the disk, where observed polarization percentages of order 20–30% indicate that the degree of uniformity of the B-field is highest, the contours of total radio emission bend outwards exactly in those areas where the strongest polarization (ordered B-field) is found. For a nonthermal spectral index of $\alpha_{\rm nth} = -1.0$, the highest possible polarization degree is 75%. Our results are consistent with particles propagating faster out of the disk along the open field lines than elsewhere (where they can only diffuse outwards at the Alfvén speed; e.g. Berezinsky et al. 1990). The overall configuration of the magnetic field lines, especially on the north-west side, where depolarization is lower than for radiation coming from the south-east (back) side, is that of an outflow cone similar to that in M 82 (Reuter et al. 1994; McKeith et al. 1995). The degree of symmetry is even higher in NGC 4666 than in M 82.

4.5. Detection of a polarized radio spur

One particularly interesting feature is the elongated area of polarized emission due west of the nuclear area, which is spatially coincident with the most conspicuous Hα line filament. This "spur" is best seen in the overlay of the map of B-vectors on-top of the Hα frame (Fig. 11). Similar polarized spurs have up to now been found in only two edge-on galaxies, NGC 4631 and M 82 (Golla & Hummel 1994; Reuter et al. 1994). The radio continuum spurs in M 82 can actually be traced back to the compact SNe and SNRs in its disk. The spur in NGC 4666 is most likely an outer wall of the central outflow cone.

The optical line ratios (see above), the distribution of soft X-ray emission (Suchkov et al. 1994), and – independently – the high degree of uniformity of the B-field and the strength of both the polarized and the total radio emission indicate that the material is compressed by shock waves propagating through the outflowing medium. We note, however, that the enhanced level of polarized emission on the ridges of the outflow cone can also at least partly be explained by projection effects. If, as envisaged by us above, the Hα filaments trace the outer walls of a cone filled with hot gas, then only a thin sheath of material on the edges might be highly polarized. The line of sight through this

Table 4. Magnetic field strengths in NGC 4666

Location	B_t	B_u	B_r	B_u/B_t	B_r/B_t
Disk	14.4	2.6	14.1	0.18	0.98
Halo	7.1	2.8	6.5	0.39	0.91

sheath is longest at the tangential points, leading to the highest signal strength (cf. Laing 1988).

As already mentioned in the context of enhanced radio continuum and optical line emission, areas outside the cone also exhibit signatures of outflows. In the area about $1'$ north of the centre this is corroborated by the high degree of alignment ($P_{\%} \simeq 20\%$) and the direction of the local B-field perpendicular to the disk (Fig. 11).

4.6. Magnetic field strengths

We estimated the line of sight averages of the field strengths of the random and regular field components in the disk and halo of NGC 4666 under the assumption of energy equipartition between magnetic field and CR energy densities and a ratio of proton-to-electron energy densities in the CRs of k = 100. This method was described e.g. by Ginzburg & Syrovatskij (1964). It should be noted, however, that it is unknown how good the assumption of energy equipartition is for galactic wind outflows.

The disk field strength is calculated from the observed radio surface brightness at 4.89 GHz which was averaged over the total radial extent of the emission as well as over the vertical range of $|z| \leq 1$ kpc, where the synchrotron emitting disk is projected onto the minor axis. Using a typical synchrotron spectral index for spiral galaxies of $\bar{\alpha} = -0.85$ (Niklas et al. 1996) and an observed disk spectral index of –0.79, we corrected the radio emission for a thermal fraction of $\sim 20\%$ at 4.89 GHz. Even then, and assuming that the typical pathlength through the disk is 4 kpc (which corresponds to an inclined synchrotron disk of 1 kpc thickness), the degree of polarization in the disk is only 3%. Such a low polarization percentage is typical for disks of edge-on galaxies (Dumke et al. 1995) and could be due either to field tangling in the turbulent ISM in the disk or Faraday effects (e.g. Burns 1966; Beck 1992; Ehle & Beck 1993).

For the halo (1.5 kpc $\leq |z| \leq$ 3 kpc, NW part only) a spectral index of $\alpha \simeq -0.90$ is observed. Hence the radio emission at 4.89 GHz in the halo is purely nonthermal. The calculated average degree of polarization is 10%, much higher than in the disk (see § 3.8). The pathlength through the halo is mostly unknown. We assume a pathlength in the range of 15–20 kpc, although the 20 kpc value might only be true for a line of sight near to the galactic disk. The main uncertainty in the calculation of the field strengths is in fact the unknown geometry (Beck et al. 1994, Berkhuijsen et al. 1996). Table 4 summarizes the estimated field strengths of the total magnetic field, B_t, the uniform component, B_u, and the random field component, B_r, in the disk and halo of NGC 4666.

The general implications are that the total magnetic field strength, B_t, in the disk is much higher than that in the halo. It falls well within the range of typical equipartition values for spiral galaxies (Fitt & Alexander 1993). The disk field is mostly turbulent. In the halo, the B-field has a higher degree of uniformity and the correlation lengths of the turbulent field might be increased. The same result was found in a study of edge-on galaxies (Dumke et al. 1995) and in NGC 253 (Beck et al. 1994). Although Berkhuijsen et al. (1996) used a different method to determine the three-dimensional structure of the regular magnetic field in the face-on galaxy M 51 and although they did not detect a vertical component of the magnetic field in the halo, it is worth mentioning that the strengths of the regular field components in the disk and halo of M 51 are comparable to those of NGC 4666.

4.7. General scenario

The observed correlation of enhanced halo emission (both optical emission line and radio continuum) with magnetic field lines perpendicular to the disk of NGC 4666 suggests that ionized matter is moving along the B-field lines during the ongoing disk-halo interaction. A similar correlation was found in NGC 891 by Dahlem et al. (1994). A natural explanation for this phenomenon is that the field is coupled ("frozen in") to the outflow of highly ionized matter. The most likely energy sources for the outflow are massive SF in the starburst of NGC 4666 and subsequent SN activity.

As predicted by Tomisaka (1992) and observed in NGC 891 and NGC 4631 (DLG95), NGC 4666 also exhibits a dependence of the structure of its (radio) halo on the level of SF in the underlying disk. The average radio continuum surface brightness and thus the SN rate in NGC 4666 is very high. Above we have shown that it is highest in the central 6.5 kpc, diminishing to about 15–30% of the maximal value in the outer disk.[3]

In the central $\sim$ 6.5 kpc, the starburst powers a bipolar outflow with an associated galactic superwind (HAM90), as discussed above. Further out in the disk the overall level of SF is lower, although locally producing enough energy for individual outflows, as visible in particular above the GEHR south-west of the nucleus. Lesch & Harnett (1993) and Lesch et al. (1990) have shown that this division of the galactic disk into two regions is connected with the galactic dynamics and its internal kinematics, in particular the location of the turnover of galactic rotation.

Our observations of the outer disk are compatible with both the "Galactic fountain" (Shapiro & Field 1976) and "chimney" model (Ikeuchi 1988; Norman & Ikeuchi 1989). In such scenarios it is envisaged that winds of OB associations blow cavities into the ambient medium over timescales of $3 \cdot 10^6$ to 10^7 years. As pointed out by various authors, magnetic fields play a crucial role in the evolution of individual SF regions. Wind bubbles of massive stars are shaped by B-fields (e.g. Chevalier & Luo 1994). At a later stage, after $\sim 10^7$ years, the stellar winds are followed (and overtaken) by the much faster SN blast waves,

[3] Using D = 26.3 Mpc here, instead of 14.1 Mpc in DLG95, which had been taken from Tully (1988), makes the supernova rate even higher than estimated by us previously.

which can finally lead to the disrupture of the gaseous disk and subsequent disk-halo outflows from the H II regions which had been partly swept free by the stellar winds (e.g. Tomisaka et al. 1981; Ikeuchi 1988). In these regions of active SF stellar winds and expanding supernova remnants produce the seed fields which are necessary to maintain galactic-scale dynamo action. Such dynamos are currently the only viable explanation for the existence of large-scale ordered magnetic fields in galaxies, which have decay times much shorter than the Hubble time (e.g. Beck et al. 1996).

4.8. Possible cause for the high-level star formation

NGC 4666 is a member of a small group of galaxies (García 1993) and it has a close companion, NGC 4668, at a projected distance of only 7′.3 (56 kpc). The difference in systemic velocities between NGC 4666 and NGC 4668 is 100 km s^{-1}. Thus, NGC 4668 might be responsible for the disturbance of the gaseous disk of NGC 4666, which is apparent in the total H I spectrum taken by Mathewson et al. (1992).

In this respect, as in many others (see above), NGC 4666 is very similar to NGC 4631, which is also disturbed by companion galaxies (Weliachew et al. 1978; Rand 1994). The central outflow cone of NGC 4666, however, is more reminiscent of M 82.

VLA H I imaging of NGC 4666 and NGC 4668 will be carried out by us in order to investigate the possibility of ongoing tidal interactions and to map the internal H I gas distribution.

5. Conclusions

We have presented evidence for a starburst driven galactic superwind in the edge-on late-type spiral galaxy NGC 4666. The outflow is visible in optical emission line imagery, radio continuum maps, and in soft X-ray images. Radio polarization data indicate that the magnetic field is following the galactic superwind on spatial scales of several kpc. The excitation conditions of the gas can be best matched with predictions from models of shock-heating. The morphology of the outflow – as seen in our multi-frequency imagery – suggests compression of the expanding material in the outer walls of the cone.

Above the outer disk of NGC 4666, although at a lower level than near the central starburst, disk-halo interactions are occurring too. This leads to individual outflows like an Hα line filament above one of the very luminous H II regions in the south-western half of NGC 4666 and also to the creation of a radio halo with a large radial extent. In general, many properties of NGC 4666 are reminiscent of NGC 4631, although the former looks less disturbed and thus more symmetric than the latter.

Acknowledgements. M. G. P. greatfully acknowledges financial support through a Summer Student fellowship granted by T. M. Heckman, C. Leitherer, and the Summer Student Program at STScI Baltimore, where the radio data were reduced. Cordial thanks to P. Kronberg for kindly providing us with the up-to-date rotation measure data for sources close to NGC 4666 prior to publication. Thanks to R.-J. Dettmar for his contributions to the radio observations. M. D. and M. G. P. thank D. Adler and E. Brinks (both NRAO Socorro) for their help in the data reduction. Many thanks also to H. Payne at STScI for his outstanding software support. We thank the referee, U. Klein, for many useful suggestions which helped to improve the paper. M. D. L. and T. M. H. would like to thank Las Campanas and CTIO observatories for the generous allocation of observing time and their staffs for expert assistance at the telescopes. The work of M. D. L. at IGPP/LLNL is under the auspices of the US Department of Energy under contract W-7405-ENG-48. M. E. is supported by the Deutsche Forschungsgemeinschaft (grant Eh 154/1-1). T. M. H. was supported in part by NASA grants NAGW-4025 and NAG5-1991. The Digitized Sky Surveys were produced at the Space Telescope Science Institute under U.S. Government grant NAG W-2166. The images of these surveys are based on photographic data obtained using the Oschin Schmidt Telescope on Palomar Mountain and the UK Schmidt Telescope. The plates were processed into the present compressed digital form with the permission of these institutions.

References

Antonucci R. R. J. & Ulvestad J. S. 1988, ApJ 300, L97
Baldwin J. A., Phillips, M. M., Terlevich R. 1981, PASP 93, 5
Beck R. 1992, IAU Symp. 157, 283
Beck R., Brandenburg A., Moss D., Shukurov A. & Sokoloff D. 1996, ARA&A (in press)
Beck R., Carilli C.L., Holdaway M.A., Klein U., 1994, A&A 292, 409
Begelman M.C., & Fabian A.C. 1990, MNRAS 244, 26P
Binette L., Dopita M., & Tuohy I. R. 1985, ApJ 297, 476
Berezinsky V. S. et al. 1990, "Astrophysics of Cosmic Rays" (V. L. Ginzburg (ed.), North-Holland, chapter 5.4
Berkhuijsen E. M. et al. 1997, A&A (in press).
Bland J. & Tully R. B. 1988, Nature 334, 43
Burns B. J. 1966, MNRAS 133, 67
Chevalier R. A. & Luo D. 1994, ApJ 421, 225
Dahlem M., Dettmar R.-J., & Hummel E. 1994, A&A 290, 384
Dahlem M., Lisenfeld U., & Golla G. 1995, ApJ 444, 119 [DLG95]
Dettmar R.-J. 1990, A&A 232, L14
Dettmar R.-J. 1992, Fund. Cosmic Phys., 15, 145
Devereux N. A., Young J. S., 1991, ApJ 371, 515
Dumke M., Krause M., Wielebinski R., & Klein U. 1995, A&A 302, 691
Ehle M. & Beck R. 1993, A&A 273, 45
Fitt A.J. & Alexander P. 1993, MNRAS 261, 445
Forbes D. A., Ward M. J., DePoy D. L. 1991, ApJ 380, L63
Fullmer L. & Lonsdale C. 1989, "Cataloged galaxies and quasars observed in the IRAS survey: version 2", JPL, Pasadena
García A. M., 1993, A&AS 100, 47
Ginzburg V. L., & Syrovatskij S. I. 1964, "The Origin of Cosmic Rays", Pergamon Press, Oxford
Gioia I. M., Gregorini L., Klein U. 1982, A&A 116, 164
Golla G. & Hummel E. 1994, A&A 284, 777
Golla G. & Wielebinski R. 1994, A&A 286, 733
Götz M., McKeith C. D., Downes D., & Greve A. 1990, A&A 240, 52
Hartigan P., Raymond J., & Hartmann L. 1987, ApJ 316, 323
Haslam C. G. T. 1974, A&AS 15, 333
Heckman T. M. 1978, Ph.D. thesis, Washington Univ., Seattle
Heckman T. M., Armus L., & Miley G. K. 1990, ApJS, 74, 833 [HAM90]
Heckman T., Lehnert M., & Armus L. 1993, in The Environment & Evolution of Galaxies, ed. J. M. Shull & H. Thronson (Dordrecht: Kluwer), p. 455

Heckman T. M., Van Breugel W., Miley G. K., & Butcher H. R. 1983, AJ 88, 1077
Hummel E., Beck R., & Dahlem M. 1991, A&A 248, 23
Hummel E. & Dettmar R.-J. 1990, A&A 236, 23
Hummel E., Lesch H., Wielebinski R., & Schlickeiser R. 1988, A&A 197, L29
Ikeuchi S. 1988, Fund. Cosmic Phys., 12, 255
Irwin J. A. 1994, ApJ 429, 618
Kennicutt R. C., 1984, ApJ 287, 116
Kennicutt R. C., Edgar B. K., & Hodge P. W. 1989, ApJ 337, 761
Kennicutt R. C. & Kent S. M. 1983, AJ 88, 1094
Kronberg P. P, Biermann P., Schwab F. R. 1981, ApJ 246, 751
Kronberg P. P, Biermann P., Schwab F. R. 1985, ApJ 291, 693
Laing R. A. 1988, Nature 331, 149
Lehnert M. D. 1992, Ph.D. thesis, The Johns Hopkins Univ., Baltimore
Lehnert M. D. & Heckman T. M. 1995, ApJS 97, 89
Lehnert M. D. & Heckman T. M. 1996, ApJ 462, 651
Leitherer C. & Heckman T. M. 1995, ApJS 96, 9
Lesch H. et al. 1990, MNRAS 242, 194
Lesch H. & Harnett J. I. 1993, A&A 268, 58L
Lynds C. R. & Sandage A. R. 1963, ApJ 137, 1005
Mathewson D. S., Ford V. L., Buchhorn M. 1992, ApJS 81, 413
McKeith C. D., Greve A., Downes D., Prada F. 1995, A&A 293, 703
Muxlow T. W. B. et al. 1994, MNRAS 266, 455
Niklas S., Wielebinski R., Klein U., Braine J., 1996, IAU 171 "New Lights on Galaxy evolution", R. Davies, R. Bender (eds.), Kluwer
Norman C. A. & Ikeuchi S. 1989, ApJ 345, 372
Osterbrock D. E. 1989, "Astrophysics of Gaseous Nebulae and Active Galactic Nuclei", University Science Books, Mill Valley, CA, chapter 12
Rand R. J. 1994, A&A 285, 833
Rand R. J., Kulkarni S. R., & Hester J. J. 1990, ApJ 352, L1
Reuter H.-P., Klein U., Lesch H., Wielebinski R., Kronberg P. P. 1994, A&A 282, 724
Shapiro P. A. & Field G. B. 1976, ApJ 205, 762
Shields J. C. & Kennicutt R. C. 1995, ApJ 454, 807
Shull J. M., & McKee C. F. 1979, 227, 131
Slavin J., Shull S.M., & Begelman M. 1993, ApJ 407, 83
Snowden S. L., McCammon D., Burrows D. N., & Mendenhall J. A. 1994, ApJ 424, 714
Sokolowski J. 1995, submitted to ApJ
Spitzer L. 1968, "Diffuse Matter in Space", John Wiley & Sons, New York
Suchkov A. A., Balsara D. S., Heckman T. M., Leitherer C. 1994, ApJ 430, 511
Sukumar S., Velusamy T., & Klein U. 1988, MNRAS 231, 765 [SVK]
Tomisaka K. 1992, PASJ 44, 177
Tomisaka K., Habe A., & Ikeuchi S. 1981, Ap&SS, 78, 273
Tully R. B. 1988, Nearby Galaxies Catalog, (Cambridge: Cambridge Univ. Press)
de Vaucouleurs G., de Vaucouleurs A., Corwin H. G., et al. 1991, Third Reference Catalogue of Bright Galaxies, (New York, Berlin: Springer-Verlag) [RC3]
Völk H.-J., Klein U., Wielebinski R. 1989, A&A 213, L12
Weliachew L., Sancisi R., & Guélin M. 1978, A&A 65, 37
Young J. S. et al. 1995, ApJS 98, 219

This article was processed by the author using Springer-Verlag LaTeX A&A style file *L-AA* version 3.